Journal of Materials Chemistry C

Accepted Manuscript

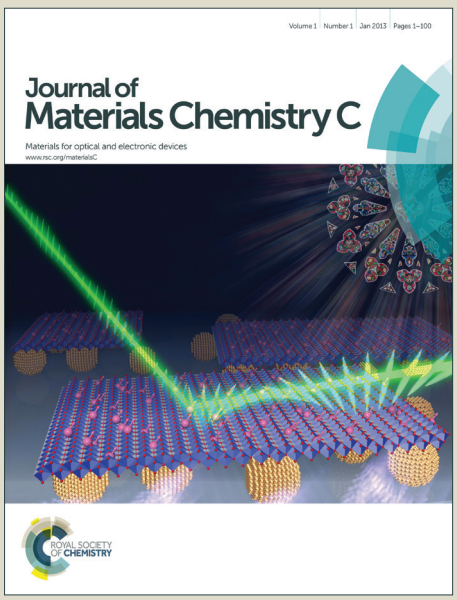

ROYAL SOCIETY OF CHEMISTRY

www.rsc.org/materialsC

Cite this: DOI: 10.1039/c0xx00000x

www.rsc.org/xxxxxx

ARTICLE TYPE

Facile Tuning of the Aggregation Induced Emission Wavelength in a Common Framework of a Cyclometalated Iridium(III) Complex : Micellar Encapsulated Probe in Cellular Imaging

Parvej Alam[a], Pradip Das[b], Clàudia Climent[c], Maheswararao Karanam[d], David Casanova[c], Angshuman Roy Choudhury[d]*, Pere Alemany[c]*, Nikhil R. Jana[b]*, Inamur Rahaman Laskar[a]*

Received (in XXX, XXX) Xth XXXXXXXXX 20XX, Accepted Xth XXXXXXXXX 20XX
DOI: 10.1039/b000000x

[a]Department of Chemistry, Birla Institute of Technology and Science, Pilani Campus, Pilani, Rajasthan, India, ir_laskar@bits-pilani.ac.in; [b]Centre For Advanced Materials, Indian Association for the Cultivation of Science, Kolkata-32, India, camnrj@iacs.res.in; [c]Departament de Química Física and Institut de Química Teòrica i Computacional (IQTCUB), Universitat de Barcelona. Martí i Franquès 1-11, 08028 Barcelona, Spain, Email: p.alemany@ub.edu; [c]Department of Chemical Sciences, Indian Institute of Science Education and Research (IISER), Mohali, Sector 81, S. A. S. Nagar, Manauli PO, Mohali, Punjab, 140306, India, angshurc@iisermohali.ac.in

Received (in XXX, XXX) Xth XXXXXXXXX 20XX, Accepted Xth XXXXXXXXX 20XX
DOI: 10.1039/b000000x

A simple synthetic protocol was developed for the syntheses of a series of monocyclometalated iridium(III) complexes involving two steps. Initially, an intermediate, $[IrHCl[(o\text{-}C_6H_3X)P(Ar)_x.(PAr_xR_y)_2]$ **[A (i, j, k, l)]**, six-coordinated iridium(III) complex involving a 4-membered chelate was isolated. Then, it was transformed into a monocyclometalated iridium(III) complex, $[(C\text{^}N)Ir(PAr_x\text{-}_1R_y)_2(Cl(H)]$ (**1-12**), through replacement of the 4-membered chelates with 5-membered cyclometalates. The intermediates and the complexes were structurally characterized by FTIR, ^1H, ^{13}C and ^{31}P NMR spectroscopies. Octahedral coordination for Ir(III) in **2, 8** and **9** was established by single crystal X-ray diffraction. Photo-physical experiments and quantum chemical calculations reveal a mixed LC/MLCT/LLCT nature for the lowest excited states all these complexes that emit bright light in the solid state. Fine tuning of the emission wavelength throughout the visible range was achieved through suitable combinations of chromophoric cyclometalates and non-chromophoric aryl phosphine ligands. More interestingly, all studied complexes were found to be aggregation induced emission (AIE) active. One of these AIE active materials (**6**) has been encapsulated inside polymeric micelles which inhibit the macroscopic precipitation of the aggregated complex, < 200 nm water soluble particle exhibiting a strong emission. These colloidal luminescent particles have been used as a potential non-toxic bio-imaging probe.

INTRODUCTION

During the last decade, there has been a tremendous interest in the scientific community to design and synthesize new luminescent materials for optoelectronic and bioimaging applications[1]. The study of fundamental photophysical properties of the emitting materials, such as exciton lifetimes, luminescence yield etc., is invariably measured in dilute solution to evade the formation of aggregated species which results in the 'aggregation caused quenching (ACQ)' effect[2] although the use of dilute solutions of these emitting species raises many issues e.g., weak emission leading to poor sensitivity in sensory systems, small number of dye molecules in the solutions that are quickly photobleached in presence of a harsh laser beam, etc[3]. The ACQ effect is, of course, an acute problem in solid state applications such as biosensor strips or organic light emitting diodes (OLEDs) because the fluorophore reaches precisely its highest level of concentration in solid state[2-3]. For this reason several strategies have been developed over the time to try to circumvent the detrimental effect of ACQ. From a chemical point of view, incorporation of branched chains, bulky cyclics, spiro kinks, or dendritic wedges have been introduced to hinder the closer approach of flat conjugated emitting molecules in concentrated solution[4]. As an alternative, in a more physical approach, the ACQ effect can be eliminated either through passivation of luminogens via surfactant encapsulation or by including them as dopants into the matrices of non-conjugated transparent polymers[5]. In both physical and chemical strategies, however, the attempts have met with limited success[6].

Instead of blocking aggregation, a natural and inherent tendency of materials, probably the best solution is to utilize this process itself to enhance light emission. A crucial step in this direction was given by Tang *et al*. in 2001, obtaining a series of silole molecules that were non-luminescent in solution while showing bright emission in solid state. This unexpected behaviour, that opens a door to the development of numerous new applications of luminescent materials, has been termed as 'aggregation induced emission'(AIE) [7]. The cause of the AIE effect in these compounds has been investigated and identified as a restricted intramolecular rotation (RIR) in the aggregates that blocks non-radiative decay, favouring in this way the radiative channels that lead to an enhanced emission. Thereafter, many new AIE active organic molecules, basically fluorescent in nature, have been designed and synthesized[4a,6,8].The AIE has also been introduced for cyclometalated complexes of iridium(III), a well-known and efficient class of triplet emitting materials, for obtaining better quantum efficiency[9]. In most of these cases, the AIE property arises due to large amplitude conformational changes of some part of the molecule that are hindered when other molecules become closer in the solid or aggregated state. For the development of new applications it would be extremely interesting to design a particular AIE active system where fine tuning of the emission wavelength could become possible. With this idea in mind, we have chosen a six coordinated iridium(III) system where two different functionalities, chromophoric cyclometalated ligands and more or less freely rotating non-planar triaryl phosphines, were connected to a single iridium(III) centre. The rotating unit are expected to show restricted intramolecular rotation (RIR) in the solid state, triggering AIE activity in these compounds. On systematic variation of the cyclometalated ligand, tuning of the emission wavelength throughout the visible range becomes possible. Here, we report a series of complexes (**1-12**) have been synthesized that emit light throughout the visible range and, more interestingly, all these complexes are found to be AIE active.

These metal complexes are soluble in organic solvents but insoluble in water and if water is added to their solution they start aggregating along with the appearance of emission.[1o] However, poor water solubility and macroscopic aggregate formation in presence of water limits their practical application. For example water soluble materials are necessary for biological labeling applications and in vitro/in vivo imaging application require good colloidal stability of the material under physicological condition along with size preferably < 200 nm size.[1m,q] Here, a simple technique has been employed for transferring these insoluble materials into water and used them as a bio-imaging probe.

EXPERIMENTAL SECTION

Materials: Iridium(III) chloride hydrate, 2-phenyl pyridine, 2-bromo pyridine, 2,4-difluoroboronic acid, palladium (0) tetrakis triphenylphosphine, triphenylphosphine, Dibenzo[f,h]quinoline benzo[h]quinoline, tris(4-(trifluoromethyl)phenyl)phosphine, methyldiphenylphosphine, dimethylphenylphosphine, 2-ethoxyethanol were purchased from Sigma Aldrich Chemical Company Ltd. 2-(naphthalen-2-yl) pyridine and 2-(naphthalen-5-yl) pyridine were synthesized by following the literature [10]. All the solvents were procured from Merck Company. PEG(1000)-b-PLA(5000) diblock polymer (MW 6000) was purchased from Polysciences, Inc.

Characterization: ^{1}H NMR, ^{13}C NMR and ^{31}P NMR spectra were recorded in a 400 MHz Brucker NMR spectroscope. FTIR Simadzu (IR prestige-21) and Perkin Elmer Spectrum 100 FTIR were used to record Infra-red spectra. UV-Vis absorption spectra were recorded in a Simadzu Spectrophotometer (model UV-1800 and 2550). Steady state photoluminescence (PL) spectra was recorded on Horiba Jobin Yvon Spectrofluorometer (FluoroMax-4). The solid state quantum yield of the thin film sample was measured using a calibrated integrating sphere in a Gemini Spectrophotometers (model Gemini 180). High-resolution MS (HRMS) were carried out with a (TOF MS ES^{+} 1.38 eV) VG Analytical (70-S) spectrometer and Q-Tof micro mass spectrometer. The size and shape of the nanoparticles were measured by scanning electron microscopy (SEM) using a JEOL JSM-6700F FESEM instrument. The hydrodynamic diameter and surface charge of the nanoparticles was measured using a Nano ZS (Malvern Instruments Ltd.) instrument. Time correlated single photon counting (TCSPC) spectra of the iridium complex in THF was obtained through exciting the sample with a picosecond diode laser (IBH Nanoled) using a Horiba Jobin Yvon IBH Fluorocube apparatus. Luminescence images of HeLa cells and photostability of the aggregated iridium complex in water and encapsulated in PEG-PLA nanoparticles were performed by drop casting the sample solution on a glass slide and images were

captured using an Olympus IX 81 microscope provided with a digital camera.

General Syntheses of Complexes:[11] To a stirred solution of $IrCl_3 \cdot 3H_2O$ (0.5025 mmol) in 2-ethoxyethanol (6 mL), substituted phosphines [triphenyl phosphine, tris(4-(tri fluoro methyl) phenyl) phosphine, methyl diphenyl phosphine and dimethyl (phenyl) phosphine] (1.507 mmol) were added and the reaction mixture refluxed at 130°C for 4-7h. Then, 2-phenyl pyridine derivatives [2,4difluorophenylpyridine, 2-phenylpyridine, benzo [h]quinoline, Dibenzo[f,h]quinoline, 2-(naphthalen-2-yl) pyridine, and 2-(naphthalen-5-yl)pyridine] (1.252 mmol) were added to the reaction mixture which was further refluxed for 3-12h. The reaction mass was brought to room temperature. The resulting solid mass was triturated and washed with hexane followed by ethanol for several times to obtain a solid (31-70%) of **1-12** that was purified through recrystallization from a mixture of DCM and hexane (1:1). X-ray quality single crystals for complexes, **2**, **8** and **9** were collected from the solution.

^{1}HNMR (400 MHz, $CDCl_3$) δ 7.57 (dd, J = 14.0, 7.5 Hz, 1H), 7.45 – 7.37 (m, 9H), 7.24 – 7.19 (m, 5H), 7.08 (dt, J = 17.0, 8.1 Hz, 12H), 6.99 (t, J = 7.5 Hz, 12H), 6.82 – 6.75 (m, 4H), -19.27 (dt, J = 29.2, 8.5 Hz, 1H); ^{13}CNMR (101 MHz, $CDCl_3$) δ 207.00, 206.95, 135.30, 135.20, 135.10, 135.05, 135.00, 132.67, 132.40, 132.16,132.13,132.06, 131.96, 129.56, 129.19, 128.57, 128.45, 127.16, 127.11, 127.06, 127.01, 126.90, 30.94; ^{31}P NMR (162 MHz, $CDCl_3$) δ 2.41, 7.54, 9.54 for A (i).IR (KBr, cm^{-1}): 2187 (m, ν_{Ir-H}) for **A (i)** (**Fig. S1**).

^{1}H NMR (400 MHz, $CDCl_3$) δ 8.11 (dd, J = 13.4, 5.4 Hz, 1H), 7.92 – 7.71 (m, 12H), 7.71 – 7.37 (m, 19H), 7.26 (d, J = 3.1 Hz, 1H), -21.58 (m, 1H).^{13}C NMR (101 MHz, $CDCl_3$) δ 136.42, 134.74, 132.55, 132.44, 125.88, 125.55, 125.03, 124.73.^{31}P NMR (162 MHz, $CDCl_3$) δ 26.39, 4.86, -24.04 for A(j). IR (KBr, cm^{-1}): 2251 (m, ν_{Ir-H}) for **A (j)** (**Fig. S2**).

^{1}H NMR (400 MHz, $CDCl_3$) δ 8.13 – 8.02 (m, 1H), 7.61 (dt, J = 8.2, 4.9 Hz, 8H), 7.50 (d, J = 6.7 Hz, 2H), 7.43 – 7.26 (m, 10H), 7.26 – 7.09 (m, 13H), 7.07 – 6.90 (m, 9H), 6.74 (td, J = 7.9, 2.1 Hz, 1H), 2.34 (t, J = 4.1 Hz, 3H), 2.15 (t, J = 4.1 Hz, 6H), -19.40 (dt, J = 17.1, 9.9 Hz, 1H).^{13}C NMR (101 MHz, $CDCl_3$) δ 135.04, 134.68, 134.48, 133.33, 133.29, 133.25, 132.23, 132.15, 131.91, 131.48, 131.22, 130.96, 130.22, 129.53, 129.43, 129.41, 128.93, 128.53, 127.99, 127.86, 127.76, 127.62, 127.48, 127.43, 127.38, 15.86, 15.65, 15.44, 11.75, 11.65, 11.55. ^{31}P NMR (162 MHz, CDCl3) δ -12.28, -40.59, -54.45 for A (k). IR (KBr, cm^{-1}): 2152 (m, ν_{Ir-H}) for **A (k)** (**Fig.S3**).

^{1}H NMR (400 MHz, CDCl3) δ 7.55 (dt, J = 7.9, 4.8 Hz, 5H), 7.35 (t, J = 7.3 Hz, 3H), 7.31 – 7.12 (m, 8H), 6.95 (td, J = 7.9, 2.5 Hz, 2H), 1.92 (t, J = 4.3 Hz, 15H). ^{13}C NMR (101 MHz, CDCl3) δ 136.23, 135.99, 130.58, 130.54, 130.50, 129.47, 129.39, 128.97, 128.54, 128.49, 128.45, 128.31, 128.21, 13.62, 13.20, 11.08, 10.88, 10.68. ^{31}P NMR (162 MHz, CDCl3) δ -40.60, -49.93 for A (l). IR (KBr, cm^{-1}): 2139 (m, ν_{Ir-H}) for **A (l)** (**Fig. S4**).

^{1}H NMR (400 MHz, CDCl3) δ 8.76 (d, J = 5.4 Hz, 1H), 7.90 (d, J = 9.6 Hz, 1H), 7.75 – 7.39 (m, 25H), 6.74 (t, J = 6.5 Hz, 1H), 6.24 – 6.02 (m, 1H), 5.75 (d, J = 8.8 Hz, 1H), -16.73 (t, J = 16.6 Hz, 1H). ^{13}C NMR (101 MHz, CDCl3) δ 149.09, 137.28,134.03, 133.97, 133.91, 133.80, 133.53, 132.69, 132.36, 132.04, 131.71, 127.55, 126.36, 124.80, 124.76, 122.48, 122.10, 121.41. ^{31}P NMR (162 MHz, CDCl3) δ 8.85 for 1. IR (KBr, cm^{-1}): 2152 (m, ν_{Ir-H}), ESI-HRMS. calculated: ($[M-Cl]^+$), m/z 1316.1242 and ($[M-H+Li]^+$): m/z 1357.1012, found: ($[M-Cl]^+$), m/z 1316.1243 ($[M-H+Li]^+$), m/z 1357.1494 for **1** (**Fig. S5**).

^{1}H NMR (400 MHz, CDCl3) 8.9 (d, 1H), 7.8 (d, J = 10.8,1H), 7.5-7.1 (m, 31H), 6.6 (t, 1H), 6.0 (t, 1H), 5.7 (d, J=13.6,1H); ^{13}C NMR (101 MHz, CDCl3) δ 149.90, 136.06, 134.02, 133.97, 133.92, 131.53, 131.27, 131.01, 129.26, 127.41, 127.36, 127.31, 126.55, 121.63, 121.46, 120.66; ^{31}P NMR (162 MHz, CDCl3) δ 7.78 IR (KBr, cm^{-1}): 2152 (m, ν_{Ir-H}), ESI-HRMS. calculated: ($[M-H]^+$), m/z 942.1609 and ($[M-Cl]^+$): m/z 908.1999, found: ($[M-H]^+$), m/z 942.1600 ($[M-Cl]^+$), m/z 908.1995 for **2** (**Fig. S6**).

^{1}H NMR (400 MHz, CDCl3) δ 8.82 (d, J = 5.3 Hz, 1H), 7.65 (d, J = 8.4 Hz, 1H), 7.61 – 7.48 (m, 4H), 7.41 (t, J = 7.6 Hz, 1H), 7.35 – 7.13 (m, 10H), 7.09 – 7.01 (m, 6H), 6.84 (d, J = 9.1 Hz, 1H), 6.73 (t, J = 6.4 Hz, 1H), 6.22 – 6.05 (m, 1H), 1.71 (t, J = 3.5 Hz, 6H), -16.71 (t, J = 15.5 Hz, 1H). ^{13}C NMR (101 MHz, CDCl3) δ 148.31, 135.91, 132.72, 132.66, 132.60, 132.49, 132.39, 132.22, 132.11, 132.06, 132.00, 129.49, 129.05, 127.77, 127.72, 127.67, 127.47, 127.42, 127.37, 122.08, 121.87, 120.84, 95.69, 14.13, 13.94, 13.76. ^{31}P NMR (162 MHz, CDCl3) δ -5.05 for 3. IR (KBr, cm^{-1}): 2152 (m, ν_{Ir-H}), ESI-HRMS. calculated: ($[M+Na]^+$): m/z 842.2687 and ($[M-HCl+2Na]^+$) m/z 828.7975,found: ($[M+Na]^+$), m/z 842.3762 and ($[M-HCl+2Na]^+$), m/z 828.9851 for **3** (**Fig. S7**).

^{1}H NMR (400 MHz, CDCl3) δ 8.85 (d, J = 5.4 Hz, 1H), 7.63 (d, J = 8.4 Hz, 1H), 7.56 (m, 1H), 7.35 (t, J = 7.4 Hz, 1H), 7.26 – 7.12 (m, 1H), 7.05 (t, J = 7.3 Hz, 1H), 7.00 – 6.84 (m, 5H), 6.74 (m, 4H), 6.38 – 6.24 (m, 1H), 1.74 (t, J = 3.7 Hz, 6H), 1.62 (t, J = 3.7 Hz, 6H), -17.87 (t, J = 18.1 Hz, 1H).^{13}C NMR (101 MHz, CDCl3) δ 147.63, 135.73, 133.69, 129.47, 128.73, 128.68, 128.64, 128.49, 128.27, 127.39, 127.35, 127.30, 121.97, 120.72, 14.79, 14.59, 14.39, 12.68, 12.49, 12.30. , 31P NMR (162 MHz, CDCl3) δ -25.62 for 4.IR (KBr, cm^{-1}): 2106 (m, ν_{Ir-H}), ESI-HRMS calculated: ($[M-H]^+$), m/z 694.0983 and ($[M+K]^+$): m/z 734.0698 found: ($[M-H]^+$), m/z 694.0977 ($[M+K]^+$), m/z 734.0695 for **4** (**Fig. S8**).

^{1}H NMR (400 MHz, CDCl3) δ 8.73 (d, J = 5.5 Hz, 1H), 7.49 (m, 26H), 7.24 (d, J = 7.0 Hz, 1H), 6.74 – 6.59 (m, 2H), 6.27 (d, J = 7.7 Hz, 1H), 6.09 – 5.98 (m, 1H), -16.72 (t, J = 16.8 Hz, 1H).^{13}C NMR (101 MHz, CDCl3) δ 165.21, 149.06, 142.87, 141.95, 136.51, 134.23, 134.05, 134.00, 133.94, 131.96, 131.63, 124.91, 124.64, 124.60, 122.20, 121.21, 118.23. ^{31}P NMR (162 MHz, CDCl3) δ 10.17 for 5. IR (KBr, cm-1): 2144 (m, ν_{Ir-H}),), ESI-HRMS calculated: ($[M-Cl]^+$): m/z 1280.1430, ($[M-H]^+$): m/z 1314.1040, ($[M-H+Li]^+$), m/z 1321.1200 and , found: ($[M-Cl]^+$): m/z 1280.1439, ($[M-H]^+$): m/z 1314.1030, ($[M-H+Li]^+$), m/z 1321.1687 for **5** (**Fig. S9**).

^{1}HNMR (400 MHz, CDCl3) 8.9 (d, J = 5.32,1H), 7.65 (d, J = 8.32,1H), 7.5 (t, J=8 ,1H), 7.4 (d, J = 7.96,1H), 7.2-7.1 (m, 30H), 6.8 (t,J=7.6, ,1H), 6.5 (t, J = 7.16,1H), 6.2 (d, J = 7.64,1H), 5.8 (t, J = 7.2,1H); ^{13}C NMR (101 MHz, CDCl3) δ 166.31, 149.61, 143.46, 135.28, 134.10, 134.05, 133.99, 132.03, 131.77, 131.51, 130.04, 128.88, 127.26, 127.21, 127.16, 122.36, 120.43, 119.21, 117.00; ^{31}PNMR (162 MHz, CDCl3) δ 9.25 for 6. IR (KBr, cm^{-1}): 2098 (m, ν_{Ir-H}), ESI-HRMS calculated: ([M-H]$^+$): m/z 906.1797, ([M-Cl]$^+$): m/z 872.2187, found: ([M-H]$^+$): m/z 906.1766, ([M-Cl]$^+$): m/z 872.2165 for **6** (**Fig. S10**).

^{1}H NMR (400 MHz, CDCl3) δ 8.62 (d, J = 5.4 Hz, 1H), 7.41 (m, 5H), 7.35 – 7.00 (m, 19H), 6.78 (t, J = 7.4 Hz, 1H), 6.64 – 6.49 (m, 2H), 1.65 – 1.59 (m, 6H), -16.74 (t, J = 15.9 Hz, 1H). ^{13}C NMR (101 MHz, CDCl3) δ 164.64, 148.24, 142.94, 135.07, 132.82, 132.76, 132.71, 132.34, 132.28, 132.23, 129.55, 128.97, 128.90, 127.43, 127.40, 123.36, 120.65, 119.75, 117.37, 14.76.,31P NMR (162 MHz, CDCl3) δ -4.57 for 7. IR (KBr, cm^{-1}): 2113 (m, ν_{Ir-H}), ESI-HRMS calculated: ([M]$^+$): m/z 783.1562, ([M-Cl]$^+$): m/z 748.1874, found: ([M]$^+$): m/z 782.9617, ([M-Cl]$^+$): m/z 748.4669 for **7** (**Fig. S11**).

^{1}H NMR (400 MHz, CDCl3) δ 8.76 (d, J = 5.5 Hz, 1H), 7.48 (d, J = 7.5 Hz, 1H), 7.32 – 7.16 (m, 3H), 7.00 (t, J = 7.3 Hz, 2H), 6.90 (t, J = 7.6 Hz, 5H), 6.81 (t, J = 7.3 Hz, 1H), 6.76 – 6.70 (m, 4H), 6.63 (t, J = 6.1 Hz, 1H), 1.79 (t, J = 3.6 Hz, 6H), 1.53 (t, J = 3.6 Hz, 6H), -17.88 (t, J = 18.4 Hz, 1H).^{13}C NMR (101 MHz, CDCl3) δ 164.57, 147.59, 142.78, 134.99, 134.34, 129.70, 128.92, 128.88, 128.83, 127.90, 127.21, 127.17, 127.13, 123.25, 120.55, 119.74, 117.37, 14.77, 14.58, 14.38, 13.34, 13.15, 12.96. 31P NMR (162 MHz, CDCl3) δ -25.45 for 8. IR (KBr, cm^{-1}): 2098 (m, ν_{Ir-H}), ESI-HRMS calculated: ([M-H]$^+$): m/z 658.1171, ([M-Cl]$^+$): m/z 624.1561, found: ([M-H]$^+$): m/z 658.0774, ([M-Cl]$^+$): m/z 624.1204 for **8 (Fig. S12)**.

^{1}H NMR (400 MHz, CDCl3) δ 9.13 (d, J = 5.1 Hz, 1H), 7.77 (d, J = 7.6 Hz, 1H), 7.54 (d, J = 8.7 Hz, 2H), 7.36 – 7.20 (m, 15H), 7.18 – 7.07 (m, 8H), 7.03 – 6.92 (m, 9H), 6.68 (d, J = 7.3 Hz, 1H), 6.46 (t, J = 7.6 Hz, 1H), -16.80 (t, J = 16.3 Hz, 1H). ^{13}C NMR (101 MHz, CDCl3) δ 154.91, 148.39, 140.42, 134.13, 133.86, 133.80, 133.75, 131.69, 131.43, 131.17, 129.46, 128.84, 128.51, 127.13, 127.08, 127.04, 125.75, 122.67, 119.86, 117.58. ^{31}P NMR (162 MHz, CDCl3) δ 10.58 for 9. IR (KBr, cm^{-1}): 2129 (m, ν_{Ir-H}), ESI-HRMS calculated: ([M-H]$^+$): m/z 930.1797, ([M-Cl]$^+$): m/z 896.2187, found: ([M-H]$^+$): m/z 930.1777, ([M-Cl]$^+$): m/z 896.2217 for **9** (**Fig. S13**).

^{1}H NMR (400 MHz, CDCl3) δ 9.20 (d, J = 5.1 Hz, 1H), 8.58 (d, J = 7.6 Hz, 1H), 8.47 (t, J = 7.0 Hz, 2H), 7.78 (d, J = 8.0 Hz, 1H), 7.67 (m, 2H), 7.36 – 7.20 (m, 13H), 7.12 (t, J = 7.3 Hz, 6H), 7.07 – 6.94 (m, 12H), 6.65 (d, J = 7.4 Hz, 1H), 6.44 (t, J = 7.7 Hz, 1H), -16.49 (t, J = 16.4 Hz, 1H). ^{13}C NMR (101 MHz, CDCl3) δ 155.93, 148.89, 141.45, 133.94, 133.88, 133.83, 131.71, 131.45, 131.28, 131.19, 130.30, 129.97, 129.39, 128.86, 128.04, 127.71, 127.17, 127.13, 127.08, 126.46, 124.15, 123.58, 122.99, 120.17, 112.72 for 10. ^{31}P NMR (162 MHz, CDCl3) δ 7.93. IR (KBr, cm^{-1}): 2113 (m, ν_{Ir-H}), ESI-HRMS calculated: ([M-H]$^+$): m/z 956.1954, ([M-Cl]$^+$): m/z 922.2342, found: ([M-H]$^+$): m/z 956.1945, ([M-Cl]$^+$): m/z 922.2349 for **10** (**Fig. S14**).

^{1}H NMR (400 MHz, CDCl3) δ 9.17 (d, J = 5.4 Hz, 1H), 8.21 (d, J = 8.6 Hz, 1H), 7.98 (d, J = 8.1 Hz, 1H), 7.74 – 7.63 (m, 1H), 7.49 (m, 2H), 7.44 – 7.30 (m, 11H), 7.28 – 6.96 (m, 19H), 6.92 (m, 1H), 6.62 (m, 1H), 6.50 (d, J = 8.4 Hz, 1H), 6.24 (d, J = 8.4 Hz, 1H), -16.30 (t, J = 16.7 Hz, 1H). ^{13}C NMR (101 MHz, CDCl3) δ 165.90, 150.46, 142.03, 135.02, 134.55, 134.55, 134.16, 134.11, 134.11, 134.05, 132.08, 131.77, 131.77, 131.46, 130.89, 130.19, 129.02, 128.97, 128.68, 127.23, 127.23, 127.18, 125.19, 121.86, 121.83, 121.48, 119.49., ^{31}P NMR (162 MHz, CDCl3) δ 6.56 for 11. IR (KBr, cm^{-1}): 2167 (m, ν_{Ir-H}),HRMS-ESI calculated: ([M-H]$^+$): m/z 980.1954, ([M-Cl]$^+$): m/z 946.2343, found: ([M-H]$^+$): m/z 980.1937, ([M-Cl]$^+$): m/z 946.2334 for **11** (**Fig. S15**).

^{1}H NMR (400 MHz, CDCl3) δ 9.08 (d, J = 5.5 Hz, 1H), 7.73 (s, 1H), 7.60 (t, J = 16.4, 7.9 Hz, 2H), 7.45 – 7.39 (m, 2H), 7.38 – 7.30 (m, 11H), 7.26 – 7.18 (m, 1H), 7.17 – 7.05 (m, 8H), 7.05 – 6.86 (m, 11H), 6.72 (t, J = 10.3, 4.2 Hz, 2H), 6.64 (s, 1H), -16.93 (t, J = 16.7 Hz, 1H). 13C NMR (101 MHz, CDCl3) δ 164.68, 160.17, 149.93, 135.31, 134.07, 134.02, 133.96, 131.70, 131.43, 131.18, 128.93, 127.72, 127.38, 127.15, 127.10, 127.05, 125.98, 124.74, 122.41, 121.33, 121.03, 117.88. 31P NMR (162 MHz, CDCl3) δ 10.17 for 12. IR (KBr, cm^{-1}): 2129 (m, ν_{Ir-H}), calculated: ([M-Cl]$^+$): m/z 922.2342, found: ([M-H]$^+$): m/z ([M-Cl]$^+$): m/z 922.2385 for **12** (**Fig. S16**).

Fabrication of thin-film on substrate for PL measurement

A 10^{-3}M solution of each of the complexes (in THF) was prepared. 2-3 drops of the solution were placed on a thin glass substrate (2x2cm^2) and the solvent was allowed to evaporate slowly.

Synthesis of iridium complex encapsulated PEG-PLA nanoparticles

PEG-PLA nanoparticles containing iridium complex were prepared using the oil-in-water based emulsion-evaporation method[12]. Typically, 15 mg PEG-PLA were dissolved in 2 mL tetrahydrofuran (THF) and mixed with 500 µL of THF solution of iridium complex (1 mg/mL). The solution was stirred for one hour and the resulting mixture was drop wise added to 15 mL water with vigorous stirring for three hours. The resulting solution was dialyzed to remove excess THF using a dialysis membrane (MWCO ~12000-14000 Da). PEG-PLA nanoparticles were also prepared following the same method without adding any iridium complex during their synthesis.

X-ray single crystal diffraction study

Single crystal X-ray diffraction data were collected on a Bruker AXS Kappa Apex II diffractometer equipped with an Oxford Cryosystem 700Plus liquid nitrogen based cooling device. The data sets were recorded at 100K using ϕ and ω scans to obtain complete data up to 60 degrees in 2θ. Data reduction and standard processing were done using the APEX II[13] suite available from Bruker AXS. Crystal structures were solved using direct methods (SHELXS97)[14] available in the Olex2[15] suite and the structures

were refined by the full matrix least squares refinement process using SHELXL97[14]. All the hydrogen atoms (except the hydride ion in **9**) were geometrically fixed at their calculated positions and refined as riding model. The hydride ion in **9** was located from the difference Fourier map and has been refined isotropically. Geometric calculations were carried out using PARST97[16].

Synthesis of aggregated iridium complexes in water

Aggregated iridium complexes in water were synthesized by drop wise addition of THF solution of iridium complex (concentration 1 mg/mL) to water with continuous sonication for 10 minutes. Excess THF was removed by dialysis using a dialysis membrane (MWCO ~ 2000 Da).

Computational Details

Geometry optimizations for complexes 2, 6 and 8-12 in their ground and lowest triplet states were carried out using quantum chemical calculations based on density functional theory (DFT) with a reparamatrization of the GGA B97 functional with an empirical dispersion correction, i.e. the B97-D functional[17]. A basis set of double-ζ quality (LANL2DZ) and the effective core potential of Hay and Wadt[18-c] were used for iridium. For all other atoms, standard all-electron 6-31+G(d)[18d] basis sets have been used. Electronic transitions to low-lying singlet and triplet states were calculated using the B3LYP[19] hybrid functional and the same basis sets. Solvation effects (Dichloromethane, ε = 8.93) were included by means of the Integral Equation Formalism – Polarizable Continuum Model (IEF-PCM)[20].The Gaussian 09 package[21]was used for all these calculations.

Cell imaging

HeLa cells were cultured in cell culture flasks and then subcultured in cell culture plates with 0.5 mL DMEM cultured media, having 10% fetal bovine serum (FBS) and 1% penicillin/streptomycin. After overnight, cells were washed with phosphate buffer solution (PBS) and then 500 µL fresh media was added. Next, 100 µL nanoparticle solution (0.7 mg/mL) was added and incubated for 1 to 8 hours. Finally, unbound nanoparticles were removed by washing with PBS buffer solution. The washed cells were then imaged under the fluorescence microscope.

MTT assay

HeLa cells were seeded into 24-well plates in 500 µL DMEM media. After 24 hours, cells were incubated with various amounts of nanoparticles. After 24 hours of incubation, media was removed and cells were washed with PBS buffer solution. Then, 500 µL fresh media and 50 µL of MTT [3-(4, 5-dimethylthiazol-2-yl)-2,5-diphenyltetrazolium bromide] solution (5 mg/mL in PBS buffer) were added to every well and incubated for additional 4 hours. Next, the supernatant was removed carefully, leaving the violet formazan in the plate. The formazan was solubilized in 500 µL 4% SDS solution of 1:1 water-DMF mixture and then absorbance was measured at 570 nm using a microplate reader. The relative cell viability was calculated assuming 100 % cell viability for a sample without nanoparticles.

3. RESULTS AND DISCUSSION

All monocyclometalated iridium(III) complexes (**1-12**) have been synthesized by a one-pot synthetic route[11]involving two steps. Initially an intermediate, $[IrHCl[(o\text{-}C_6H_3X)P(Ar)_{x\text{-}1}Ry](PAr_xR_y)_2]$ [**A (i, j, k, l)**] (**Scheme 1**) was isolated in which a six fold coordination environment on iridium(III) involving a 4-membered chelate was formed. It was observed that the time required to obtain the intermediates when using trifluoro methyl phosphine (**j**) or dimethyl phenyl phosphine (**l**) were relatively longer (~7h) than for the other two intermediates with triphenyl phosphine or diphenyl methyl phosphine (~4h; **Table S1**). The presence of Ir-H in the intermediates **A** is supported by the observation of a stretching frequency in the region~2187-2252 cm^{-1} recorded by FTIR and by the appearance of high-field lines in the ^1H NMR spectra. Although the hydroxylic solvent, 2-ethoxyethanol[22] seems at a first sight to be the most plausible source of hydrogen linked to iridium(III), the same intermediate (**A**) was formed when the reaction was carried out in a non-hydroxylic solvent (1,4-dioxane). The measured ratios of the integrated areas of the high-field lines (for hydride linked to Iridium) vs aromatic proton resonances were 1 to 50 ± 5 **(i-l)**

Scheme 1

The synthetic route for the monocycometalated iridium(III) complexes B (**1-12**) via intermediates **A (i, j, k, l).**

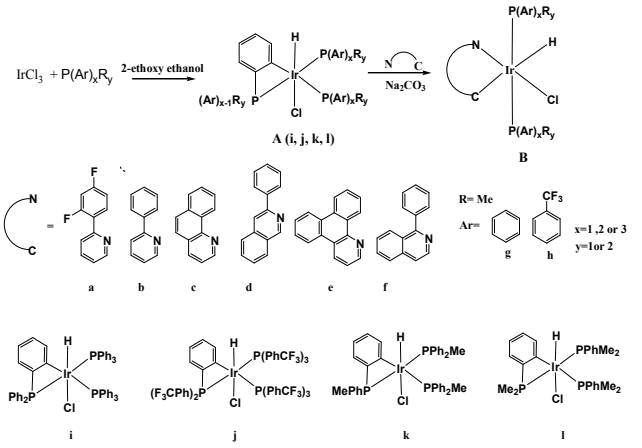

Comp.		Ar	x	y	Comp.		Ar	x	y	Comp.		Ar	x	y
1	a	h	3	0	**5**	b	h	3	0	**9**	c	g	3	0
2	a	g	3	0	**6**	b	g	3	0	**10**	d			
3	a	g	2	1	**7**	b	g	2	1	**11**	e			
4	a	g	1	2	**8**	b	g	1	2	**12**	f			

(Calculated for a mono hydride, 1 to 44), showing that one hydrogen atom was abstracted from the ligand[23]. The only reasonable source for the hydrogen atom which migrates to the iridium(III) centre is the ortho hydrogen adjacent to phosphorous, resulting in a six fold coordination of iridium(III) with a strained 4-membered chelate ring[23]. In the second step, the 4-membered chelate ring in the intermediates **(i-l)** is replaced by the stable 5-membered cyclometalates to form six-coordinated monocyclometalated iridium(III) complexes (**B**, **1-12**) (**scheme 1**). The yield of the product has been improved in the range of 10-15%, on carrying out the process in presence of 3-4 equivalents of sodium carbonate, which is acting as an acid scavenger (**Table S1**)[24]. The observed chemical shift (δ) in the range of (-15) – (-19) and their low coupling constants (J_{P-H}, 16.0-18.5) (**Table 1**), support the existence of hydride bonded to iridium(III) and cis configuration with respect to phosphorous coordinated species (PAr_3) in the complex molecule, respectively. The structure of the complexes **2**, **8**, and **9** is established by X-ray single crystal analyses at 100K.

Table 1 The IR, ^{1}H NMR (for hydride only) and ^{31}P NMR support the presence of a Ir-H bond and phosphorous coordination, respectively for **1-12**

Complex	IR $\nu_{(Ir-H)}$	^{1}HNMR(hydride) ppm	^{31}P NMR Ppm
1	2152	-16.73(J=16.8Hz)	8.85
2	2152	-16.76(J=16.8Hz)	7.78
3	2152	-16.71(J=16.8Hz)	-5.05
4	2106	-16.87(J=16.8Hz)	-25.62
5	2144	-16.72(J=16.8Hz)	10.17
6	2090	-16.71(J=16.8Hz)	9.25
7	2113	-16.74(J=16.8Hz)	-4.57
8	2098	-16.88(J=16.8Hz)	-25.45
9	2129	-16.80(J=16.8Hz)	10.58
10	2167	-16.30(J=16.8Hz)	6.56
11	2113	-16.49(J=16.8Hz)	7.79
12	2129	-16.93(J=16.8Hz)	10.17

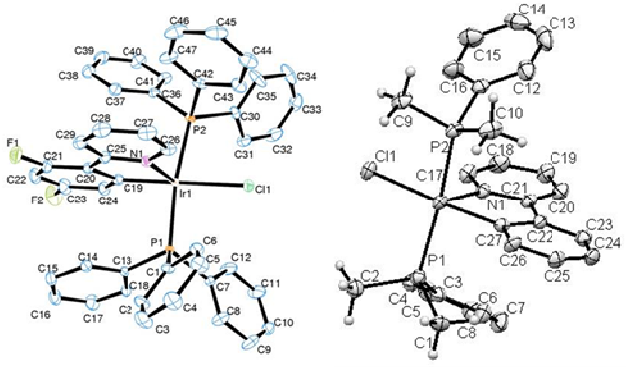

2 **8**

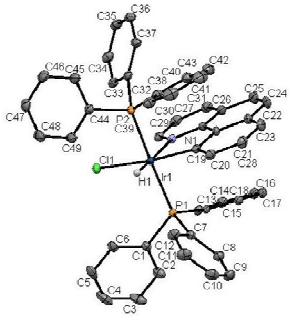

9

Fig. 1 ORTEP diagram for complexes, **2**[10], **8** and **9** showing the octahedral geometry at the Ir site (in **2** and **8**, the hydride coordination to Ir(III) centre couldn't be detected).

Due to the poor X-ray scattering factor of the hydride ion, in **2**, one coordination site around Ir appears to be empty although this position is certainly occupied by the hydride ion as supported by the IR and ^{1}H NMR spectra. The ORTEP diagram (**Fig. 1**) shows an octahedral geometry for the coordination environment around the iridium(III) centre for **2**, **8** and **9**. Crystallographic data and selected geometrical parameters are given in **Tables S2-S3** for all three structures. Also, the most significant geometrical parameters for the optimized ground state and lowest triplet structures in DCM solution are given in Tables S4 and S5, respectively. All optimized structures are very close to the X-ray geometries. Remarkably, the main difference between crystallographic coordinates and geometries obtained from quantum chemical calculations are found in the disposition of the phenyl rings in the phosphine legands, which can be explained considering the expected greater molecular flexibility of these ligands in solution (**Fig. S17**).

The solution UV-Vis absorption spectra (DCM, 10^{-5}M) show intense bands below 350 nm for the complexes, **1-12** [**Fig. 2, S17**] which can be assigned to ligand centered (LC), $^1\pi$-π^* transitions[25]. These absorption bands are followed by weaker bands in the range of ~350-450nm. In this range, two well-resolved broad peaks are observed for **1-9** [inset of (**Fig. 2, S18**)] whereas a single broad peak is obtained for **10-12**. Based on the shape, band position and their intensities [**Table 2**][24] these bands can be assigned to MLCT transitions. Electronic structure calculations of complexes **2**, **6** and **8-12** indicate that the four highest occupied molecular orbitals (HOMOs) correspond to different antibonding combinations between the t_{2g} (d_{xy}, d_{xz} and d_{yz}) orbitals of iridium 'p' orbitals of chlorine and π contributions from the non-pyridine rings of the cyclometalated ligand, while the two lowest unoccupied orbitals (LUMO and LUMO+1) correspond to π* orbitals of the cyclometalated ligand (**Fig.3**).There is almost no participation of the phosphine ligands in these frontier orbitals. Our TDDFT computations suggest that the highest wavelength, weak bands correspond to spin-forbidden transitions to low-lying triplet states resulting from HOMO and HOMO-3 to LUMO electronic excitations (**Table 3**). In all studied complexes, the lowest energy spin-allowed absorption band corresponds to the promotion of an electron from the HOMO to the LUMO, and presents an important MLCT and

LLCT, i.e. p(Cl) →π*, character (**Fig. 3**). Complexes **6** and **8** only differ in the phosphine ligand and, as a result, their transition energies to S_1 are almost identical. On the other hand, fluorine substitution in **2** destabilizes the π*-type LUMO, resulting in a ~0.1 eV increase of the excitation energy. Alternatively, modification of the degree of conjugation in the cyclometalating ligands in **9**, **10**, **11** and **12** can be used to tune the S_0→ S_1 transition energy almost at will. Details on the transition energies, oscillator strengths and orbital composition of the lowest singlet and triplet states can be found as Supporting Information (Table S6). Overall, computed transition frequencies to the low-lying states of the complexes are in very good agreement with experimental absorption peaks in dichloromethane solution.

The emission spectrum of complexes, 1-10 shows a structured emission (**Fig. S19**). Further, these complexes are insensitive to solvatochromic effects *i.e.*, the emission spectra remain practically unchanged irrespective of the polarity of the solvent (**Fig. S20**). These facts suggest that the lowest excited states of **1-10** are of predominantly LC character along with a lesser contribution from MLCT states. This behaviour is also nicely captured by electronic structure calculations. The comparative analysis between the S_1 and T_1 wave functions shows a much lower weight of the HOMO-to-LUMO (MLCT) for the latter (Table 3). In particular, the lowest triplet wave function has an important participation of the HOMO-3, largely located on the cyclometalled ligand (**Fig.3**), hence increasing the LC nature of the triplet.

Table 2 UV-Vis absorbance [extinction coefficient ($M^{-1}cm^{-1}$) in parenthesis] and maximum emission wavelengths for the complexes **1-12**

Complex	UV-Vis absorbance (nm)(Ɛx10^4) (M^{-1} cm^{-1})	PL (nm)	
		Solid	Solution
1	268 (9.00), 350(1.60), 430(0.15)	441 (sh), 472, 506 (sh)	445,471
2	255 (23.50) 338 (2.30), 369 (1.50), 430(0.05)	448 (sh),476, 507 (sh)	451,476
3	255 (2.80), 339 (1.70), 367 (1.00), 419 (0.02)	443 (sh), 478, 507 (sh)	453,475
4	262 (4.10), 337 (0.51), 369 (0.33) 419 (0.05)	481	448,476
5	275 (13.10), 371 (1.70), 430(0.05)	460 (sh), 493, 529 (sh)	463,494
6	269 (5.30), 343 (0.65), 381 (0.51),445 (0.02)	473,498	468,499
7	260 (29.45), 347 (2.87), 385 (2.30), 430 (0.02)	473 (sh), 501	467,497
8	259 (35.20), 349 (3.60), 384 (2.70), 430 (0.02)	475, 507	468,497
9	276 (7.60), 407 (0.71), 451(0.04)	508, 544	512,548
10	280 (13.00), 319 (5.50), 336 (5.10), 424 (0.59)	513, 558	543,585
11	254(12.30), 267(10.70), 331(1.86), 400 (0.27)	548, 610 (sh)	524
12	275(6.7), 336(0.96), 423 (0.40)	593	589

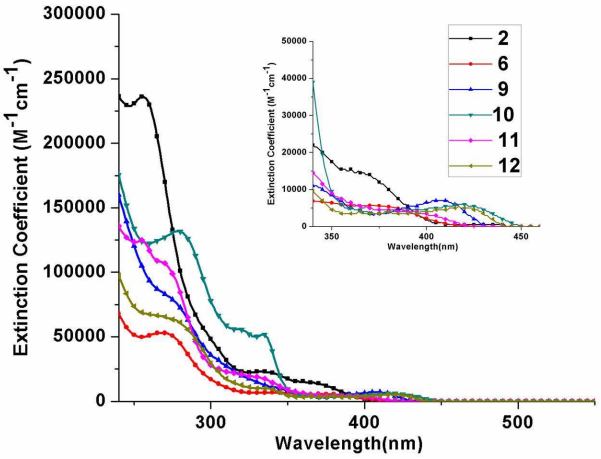

Fig. 2 Solution UV-Vis absorbance spectra (10^{-5}M, DCM) of the complexes, **2**-**12** [short range spectrum are shown in inset (360-460 nm)].

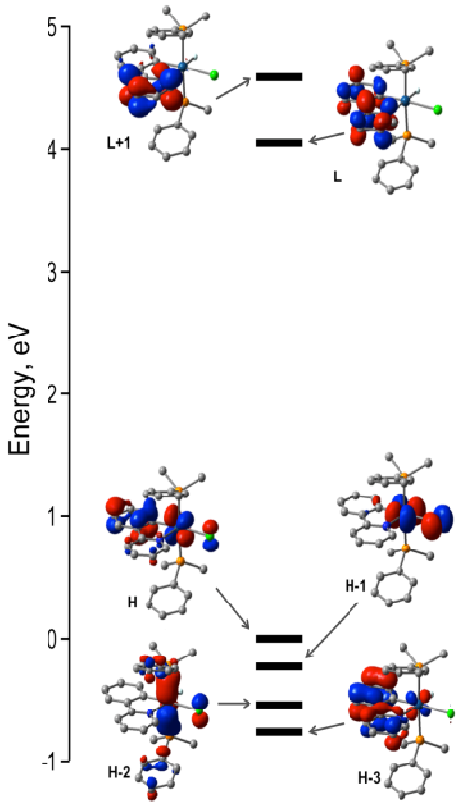

Fig. 3 Molecular orbital energy diagram (in eV)with respect to the HOMO energy of the frontier orbitals of **8**. H and L stand for HOMO and LUMO, respectively.

Table 3. Comparison between experimental absorption maxima λ_{exp} and computed transition energies λ_{calc} (in nm) and orbital composition (%) of the lowest excited singlet and triplet states for complexes **2**, **6** and **8-12**.[a]

Complex	state	λ_{exp}	λ_{calc}	H→L	H-n→L[b]
2	T_1	430	433	56	25
	S_1	369	360	97	
6	T_1	445	451	68	19
	S_1	381	372	97	
8	T_1	430	445	68	21
	S_1	384	368	97	
9	T_1		494	47	13
	S_1	407	400	94	
10	T_1		553	63	16
	S_1	424	418	94	
11	T_1		465	28	17
	S_1	400	393	95	
12	T_1		567	84	
	S_1	423	419	84	

[a]complementary for higher singlet and triplet states can be found as Supplementary Information (**Table S6**). [b]Contribution from H-n with 1 ≤ n ≤ 3 (see **Table S6**).

The emission color of the complexes has been tuned throughout the visible range by changes in the cyclometalated ligands / or combinations of cyclometalated and phosphine ligands (**Fig. 4**). The relative differences in the emission wavelengths for the studied complexes are well recovered by computational results (**Table S7**). It is to be noted that a sharp change of color is observed with the variation of the cyclometalated ligands, where as a minor effect is reflected for changes in the phosphine ligands (**Fig. 4**), which is in line with the low electron population on the phosphine ligands for the frontier molecular orbitals involved in the electron transition (**Fig. 3**). Inclusion of a trifluoro methyl substituent in triphenyl phosphine (**1** vs **2**; **5** vs **6**) has a negligible influence in the emission wavelength (**Fig. 5**, **S20**). Similarly, the complexes with methyl or dimethyl substituted tri phenyl phosphine (**3** vs **4**; **7** vs **8**) show only minor variations in the emission wavelength (**Fig. 5**, **S21**). There is, however a noticeable difference in color comparing complexes **1** and **2** with **3** and **4** (a similar change is observed when comparing **5** and **6** with **7** and **8**, **Fig. 4**) where the phenyl groups from phosphine are replaced by one or two methyl groups. In these cases, it is evident that the phosphorous atom coordinating to iridium(III) affects its d-orbitals when the electron accepting phenyl substituents are replaced methyl groups in the triphenylphosphine ligands.

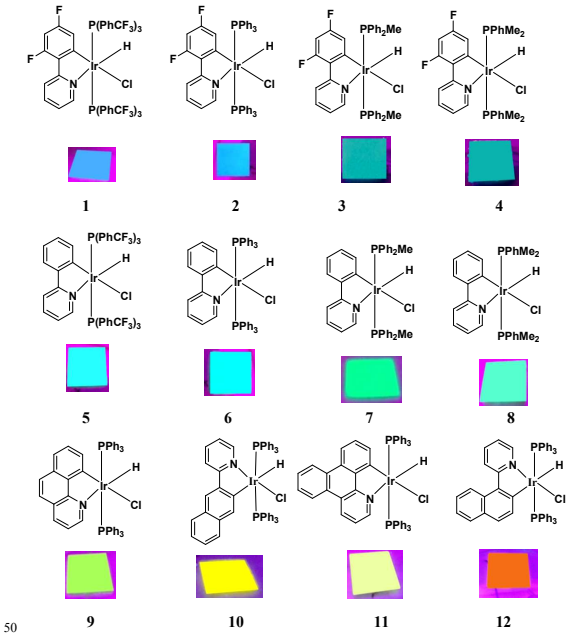

Fig.4 Tuning of emission color in solid state throughout the visible range with variation of the cyclometalated and the phosphine ligands.

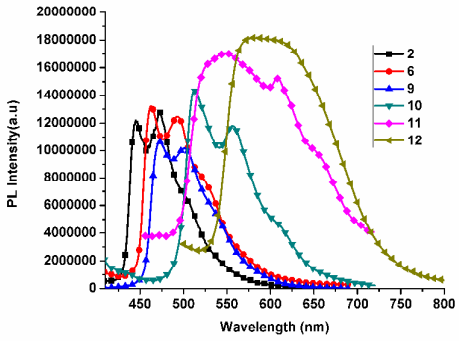

Fig. 5 Solid state photoluminescence emission spectra for complexes **2-12**, showing the tuning of emission wavelengths.

The photoluminescence (PL) intensity of all these complexes in dichloromethane was found to be very weak as compared to their respective solids / aggregated forms (**Fig. 5, 6**).

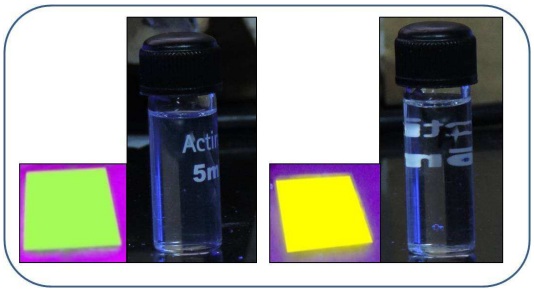

Fig.6 The relative luminescence intensity of solid state vs. solution for complexes **9** (left) and **10** (right) under UV lamp (λ_{max} = 365nm). (These are chosen as two representative cases of all the reported complexes).

Table 4 Solid state quantum efficiency (ϕ_{solid}) and solution state quantum efficiency (ϕ_{sol}) for **1-12**

complex	ϕ^a_{sol}	ϕ^b_{solid}	complex	ϕ^a_{sol}	ϕ^b_{sol}
1	0.011	5.41	7	0.015	9.46
2	0.890	41.43	**8**	0.048	7.28
3	0.014	10.65	**9**	0.044	9.14
4	0.127	10.95	**10**	0.114	26.4
5	0.014	5.77	**11**	0.012	7.99
6	0.688	54.83	**12**	0.087	11.42

[a]Solution QE (ϕ_{sol}) for **1-10** has been measured with respect to quinine sulfate (in 0.1M H_2SO_4, QE=0.55, excitation,470nm-480nm); and QE (ϕ_{sol}) for 11-12 has been with respect to coumarin 153 (in degassed ethanol, QE=0.38, excitation, 400-420nm), Solid state phosphorescence QE (ϕ_{solid}) has been recorded using integrating sphere.

The quantum efficiencies in solution of the complexes have been measured and the observed values are in the range, 0.01-0.89 (for **1-10** measured with respect to quinine sulphate in 0.1M sulphuric acid, quantum yield (QE) = 0.55, Table 4) and 0.012 and 0.087 for complexes **11** and **12**, respectively (with respect to coumarin 153 dissolved in degassed ethanol, QE = 0.38, Table 4). The least solution efficiency was observed in **1** (0.011%) while the maximum efficiency in **2** (0.89%). The absolute solid state QE has been measured[26] for all the complexes. The maximum QE was observed for **2** (54.83%), while the minimum observed for **1** (5.41%). The ratio of QE_{solid} / QE_{sol} (ϕ_{solid}/ϕ_{sol}) has been found maximum for **3** (7.34×10^2) and minimum for the case of **2** (0.46×10^2) showing the remarkable AIE property of the complexes.

Several experiments have been carried out in order to investigate the cause of the strong solid state emission behaviour exhibited by complexes **1-12**. PL was measured for a series of solutions with different water-THF ratios, in which water content was gradually varied in the range of 0-90% for **1-12**. The PL was

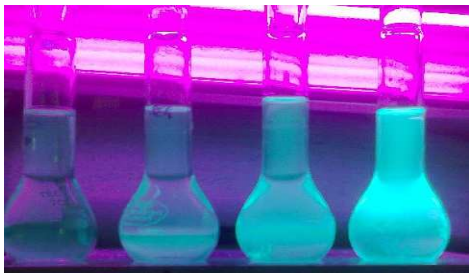

a

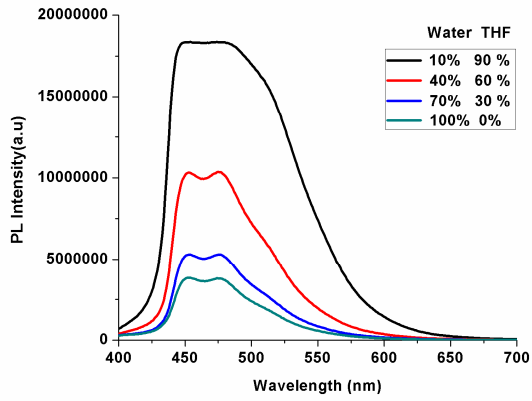

b

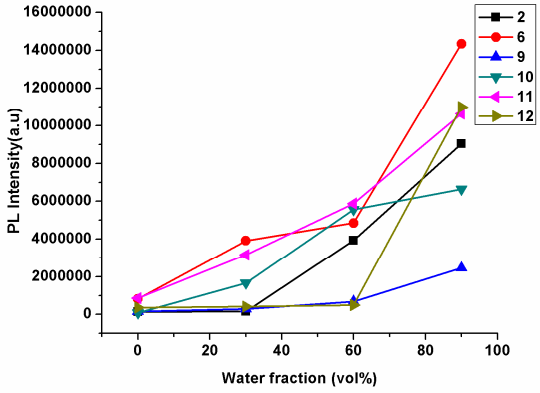

c

Fig. 7 (a) Luminescent image of complex **4** radiated with an UV light at 365 nm in water–THF mixed solvents (0, 30, 60 and 90% water into THF solution) with the concentration $1x10^{-4}$ mol.L^{-1}; **(b)** PL spectra of complex **4** in different water–THF mixed solvent (0, 30, 60 and 90% into THF solution); (**c**) change in PL intensity of complexes **2, 6, 9, 10, 11** and **12** with changing the water fraction.

a

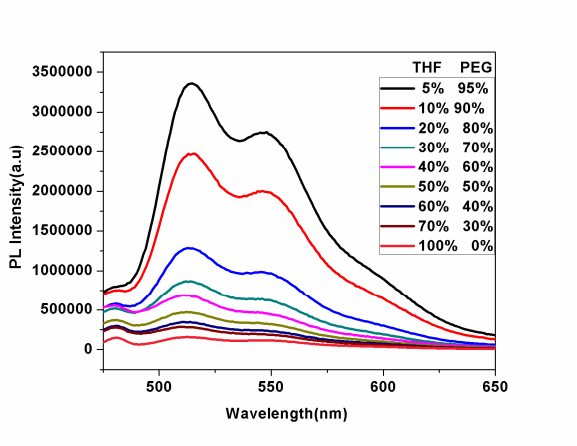

b

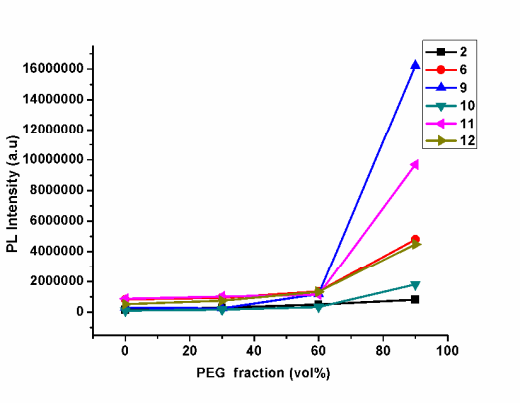

c

Fig. 8 (a) Luminescent image of complex **9** radiated with an UV light at 365 nm in PEG–THF mixed solvents (0, 30, 60 and 90% PEG into THF solution) with the concentration 1x10^{-4} mol.L^{-1}; **(b)** PL spectra of complex **9** in different PEG–THF mixed solvent (0- 95 % PEG into THF solution); (**c**) change in PL intensity of complexes **2, 6, 9, 10, 11** and **12** with changing the PEG fraction

found to increase drastically with increasing proportion of water in a water-THF solution (**Fig. 7, S22a**). Since water is a poor solvent for all these complexes, the molecules aggregate with increasing concentration of water. Micrometer size non-uniform aggregated particles have been observed in the SEM image for complex **6** in 90% water-THF solution[11]. Thus, this experiment indicates that all these complexes are aggregation induced emission (AIE) active. In another experiment, the gradual increase of the emission intensity is observed with increasing the concentration of polyethylene glycol, a viscous solvent, in a solution of each of the complexes **1-12** dissolved in THF (**Fig. 8, S22b**). This fact suggests that the hindrance of the rotationally active part with increasing viscosity of the solution may be responsible for the increase of luminescence intensity in aggregated samples. Finally, the AIE effect for complex **6** (as a representative of all other complexes) was studied by the time-resolved photoluminescence technique (**Table 5**, Fig**. 23S**) [4a,27] In THF, the molecules decay bi exponentially (95% molecules decay with life time 2.17 ns and the rest decay with lifetime 43.39 ns). With addition of water (30%) into THF, excited molecules decay through three different relaxation pathways (13% and 10% molecules decay with life

Table 5 Luminescence decay parameters for the complex 6 solution at 298K[a].

No.	Solvent	A_1(%)	A_2(%)	A_3(%)	τ_1(ns)	τ_2(ns)	τ_3(ns)
1	THF	95	5	------	2.17	43.39	-----
2	THF-H_2O (30%)	13	10	77	2.00	5.59	484.14
3	THF-H_2O (60%)	8	1	91	2.18	42.69	642.39
4	THF-H_2O (90%)	5	4	91	2.03	92.60	4556.59

[a]These parameters were determined from the equation, I =A1exp (-t/τ1) + A2exp(t/τ2) for the solution 1 and for the rest of the solutions (2-3) from the equation, I =A1exp(-t/τ1) + A2exp(t/τ2) + A3exp(-t/τ3) where A and τ, represents the fractional amount and the life time of the shorter, medium and the longer species, respectively

times of 2 ns and 5.59 ns, respectively, but 77% of the molecules decay through a slow channel with a life time ~484ns). With further addition of water molecules (60%) in THF, the decay *via* the slowest channel is more populated (from 77% to 91%) and the life time increases to ~642ns. In 90% water, the life time for the slowest component rises to ~4.6 μs, without any noticeable change in population (60%). It has been observed that the lifetime for the new relaxation pathway is steadily rising (with population, too) when the concentration of water molecules is increased. This fact leads us to propose that restricted intramolecular rotation (RIR) can affect drastically the radiative/nonradiative recombination processes in the excited states.

The packing diagrams for complexes **2**, **8** and **9** shows that there are several intermolecular interactions where phenyl rings in the triphenyl phosphine units are involved (**Fig. 9**). Thus, the internal rotation of these rings is severely restricted in the crystals. This fact is also consistent with the geometry optimizations using quantum chemical calculations that show that in solution the minimum energy disposition of those phenyl rings is markedly different to that adopted in the crystal structure (**Fig. S17**).This hindered rotation of the phenyl rotors in the crystal state is suggested to block the non-radiative decay channels while simultaneously opening the radiative pathways. As a result, the solid state emission efficiency for all these complexes is predicted to improve significantly, as observed experimentally.

Application in cell imaging

As an illustration of possible applications for these new AIE active complexes we have employed them in the design of a non-toxic bioimaging probe. Since these complexes are soluble in tetrahydrofuran and dichloromethane but insoluble in water, a polyethylene glycol-polylactic acid (PEG-PLA) based biodegradable polymer has been selected that is known to self-assemble in water and produce a micellar structure with hydrophobic PLA inside and hydrophilic PEG outside[28] in which the AIE active Ir(III) complexes can be encapsulated. In our

experiment, complex **6** has been used for bioimaging as probe molecule. Micellar encapsulation of AIE active iridium complexes involves solubilization of a mixture of PEG-PLA and the iridium complex in the organic solvent followed by injection of this mixture in water under vigorous stirring conditions to favour self-assembly of PEG-PLA into micelles that incorporate the iridium complex in its aggregated form (**Scheme 2**).

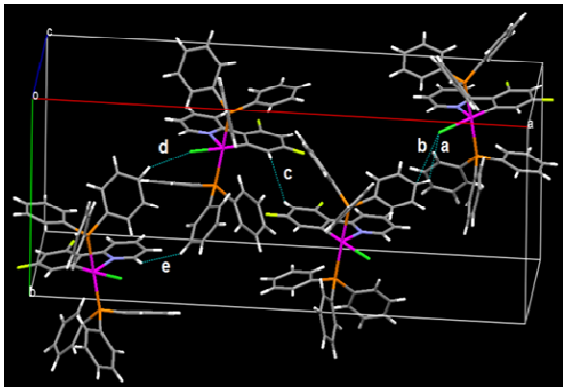

a

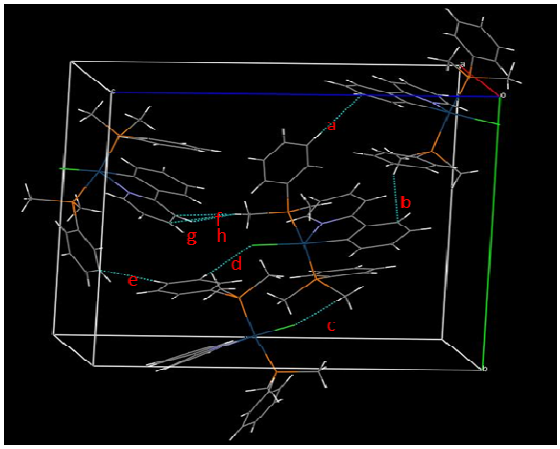

b

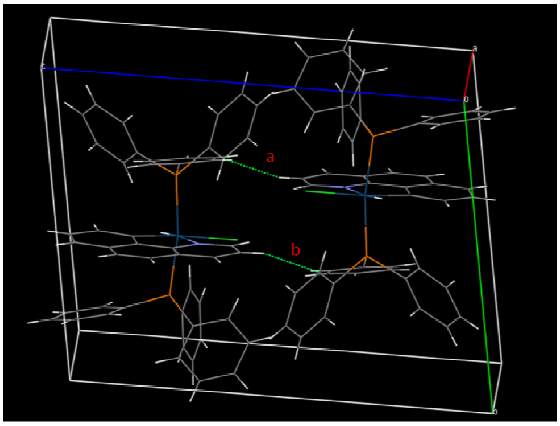

c

Fig. 9 Packing diagram for **2** (a), **8** (b) and **9** (c); in **2** the unit cell contains four molecules and the green dotted lines denote the shortest contacts (a = 2.88 Å; b = 3.42 Å; c = 2.71 Å, d = 2.95 Å and e = 2.70 Å); in **8** the unit cell contains four molecules (a = 2.73 Å; b = 2.86 Å; c = 2.93 Å, d = 2.84 Å , e = 2.84 Å, f=2.38Å,g=2.77 Å, h=2.88 Å); in **9** the green dotted lines denote the shortest contacts(a=b=2.86 Å).

Scheme 2 Schematic representation of the synthesis of luminescent iridium complex encapsulated PEG-PLA nanoparticles.

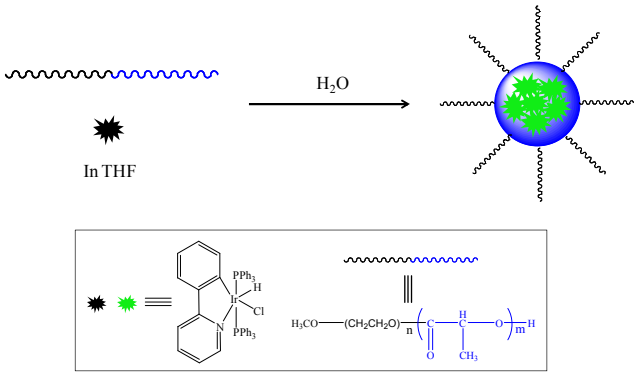

The PL properties of **6** dissolved in THF, in its aggregated form in water and in a PEG-PLA colloidal solution after encapsulation in PEG-PLA micellar nanoparticles are shown in **Fig.10** and in the supporting information (**Fig. S24**). The iridium complex in THF shows a weak green emission under 365nm excitation with the maximum emission at 470 nm and 495 nm. The aggregated iridium complex in water and encapsulated in PEG-PLA

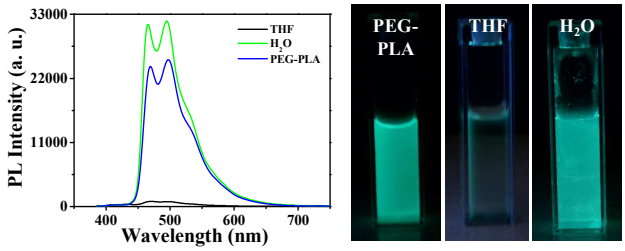

Fig. 10 Photoluminescence spectra (left) and digital image (right) of iridium complex **6** in Tetrahydrofuran (THF), water and in aqueous.

micellar nanoparticles shows strong green emission under excitation at 365 nm with two emission maxima at (465 nm, 495 nm) and (470 nm, 495 nm), respectively (**Fig. S24**). The observation of a similar strong green emission in water and PEG-PLA micelles indicates that the iridium complex is in its aggregated form inside the PEG-PLA micelles.

Aggregation and particle formation of the iridium complex in water is also confirmed from dynamic light scattering (DLS) and scanning electron microscope (SEM) measures as shown in **Fig. 11**. The hydrodynamic diameter of the particles of aggregated complex as determined by DLS ranges from 200 nm to 900 nm. The SEM image shows that the particles of aggregated complex in water have diameter ranging from 50 to 400 nm with a spherical shape (**Fig.11**). These results confirm that the iridium complex aggregates in water to give micron size particles with a wide size distribution (**Fig. 11** and **Fig. S25**). In contrast, the hydrodynamic size of PEG-PLA nanoparticles and iridium complex encapsulated PEG-PLA nanoparticles are 35-150 nm and 65-220 nm,

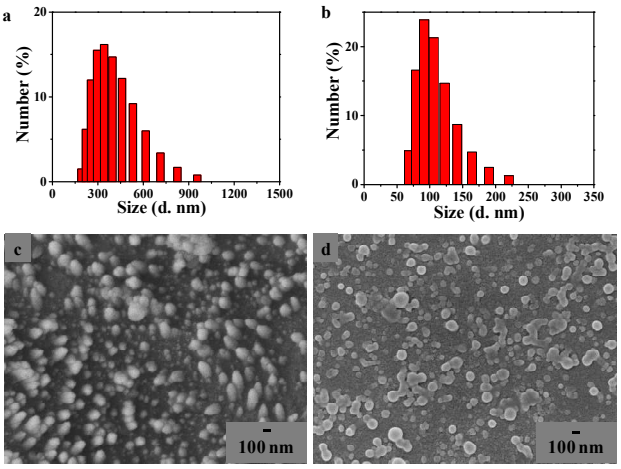

Fig. 11 DLS histogram (a, b) and SEM image (c, d) of aggregated iridium complex (**6**) in water (a, c) and PEG-PLA particles encapsulated with iridium complex (b, d). Note the comparative smaller size and narrow size distribution of PEG-PLA particles.

respectively (**Fig. 11**, **S25**). A SEM study also confirms that the iridium complex encapsulated PEG-PLA nanoparticles are spherical in shape with radii in the range 40-150 nm (**Fig. 11**). These results confirm that PEG-PLA particles containing the complex in its aggregated form are smaller than the particles of pure aggregated iridium complex in water with a relatively narrow size distribution for the encapsulated particles. The size of the micelle is found to increase by about 30 to 70 nm after the encapsulation of iridium complex takes place.

The presence of iridium complex inside the PEG-PLA particles is confirmed from IR spectroscopy. The FTIR spectrum for the isolated iridium complex shows that the major characteristic peaks arise at 2092 cm^{-1} for Ir-H stretching and 3046 cm^{-1} for aromatic C-H stretching[11]. The spectrum for PEG-PLA nanoparticles shows peaks at 2955-2850, 1752 and 1180 cm^{-1} which are characteristic of C-H stretching, C=O stretching and C-O stretching, respectively[29]. In the spectra for PEG-PLA particles including iridium complex vibrational peaks at 2085 cm^{-1} and 3046 cm^{-1}corresponding to the iridium complex and those corresponding to the PEG-PLA are both present (**Fig S26**). Further, SEM based elemental mapping experiment of iridium complex encapsulated PEG-PLA particles demonstrate that iridium complex lying inside of PEG-PLA nanoparticles (**Fig S27**). A PL decay study shows that the lifetime of iridium complex in THF, water and PEG-PLA is 5.1 ns, 6.3 µs and 19.8 µs, respectively (**Fig. S28**). Magnitudes of the same order for the lifetimes of the aggregated iridium complex in water and inside the PEG-PLA micelles demonstrate that in both cases the emitting molecules are found in similar micro environments which are notably different from those in THF solutions[30]. The stability of the emission of the aggregated iridium complex under continuous UV irradiation has been tested finding that the iridium complex is stable under UV irradiation for more than a minute (**Fig. S29**). This result suggests that the emission of PEG-PLA particles containing the iridium complex is stable under imaging conditions and can be thus used as imaging probes.

Micelles of PEG-PLA encapsulated AIE active iridium complex have been used as in vitro cellular imaging probes for biomedical applications. For this purpose HeLa cells have been incubated with luminescent PEG-PLA particles and then labelling has been observed under a fluorescence microscope. The results show that the cells become green luminescent under UV excitation as

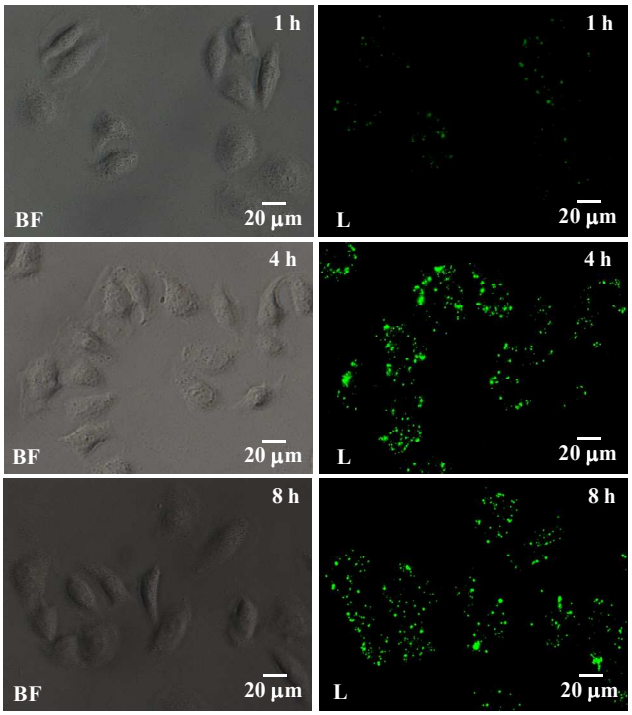

Fig.12 Bright field (BF) and luminescence (L) image of HeLa cells labelled with iridium complex (**6**) encapsulated PEG-PLA particles. Cells are incubated with particles for 1, 4 and 8 hours and then washed cells are imaged under microscope.

shown in **Fig.12**, suggesting that the particles can be used to label them. As shown in Fig. 12, by varying the incubation time, it's difficult to understand whether particles enter into the cytoplasm even after an 8 hours exposure. So, we have performed a series of fluorescence images at different Z planes with particle labeled of HeLa cells, demonstrating that the particles are located in cytoplasm along with at cell surface (**Fig. S30**). Interestingly, particles of iridium complex aggregated in water do not label the cells even after a long incubation time (**Fig. S31**). This result suggests that successful labeling by photoluminescent PEG-PLA particles is possibly due to their smaller size combined with the lipophilic property of PEG-PLA that leads to a strong interaction of the particles with the cell membrane[31]. Encapsulated PEG-PLA nanoparticles were mixed with Dulbecco's modifed eagle medium (DMEM) with 10% fetal bovine serum (FBS) to check their stability. The observed digital images of these particles in cell culture medium indicate that there has no significant precipitation till 7 days (**Fig. S32**) which ensures colloidal stability of iridium complex encapsulated PEG-PLA particles in cell culture media. The cytotoxicity of the iridium complex has been investigated by the conventional MTT assay. HeLa cells are incubated with various amounts of photoluminescent PEG-PLA

particles for 24 hrs and cell viability has been estimated. Result shows that cells survival is >80% in all the tested concentrations (**Fig**. **13**). This result suggests that photoluminescent PEG-PLA particles have low toxicity and can be used as cell imaging probes under in vitro conditions.

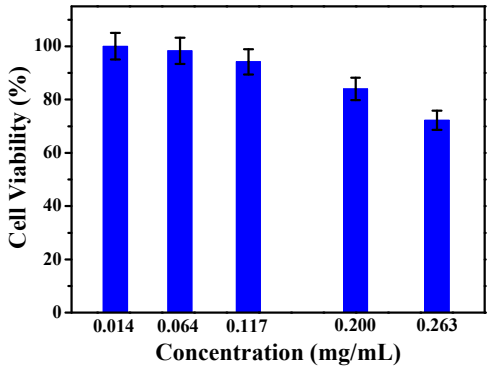

Fig. 13 Viability of HeLa cells in presence of iridium complex (**6**) encapsulated PEG-PLA nanoparticles. Cells are incubated in presence of different concentrations of iridium complex encapsulated PEG-PLA nanoparticles for 24 hours. (The final concentration of iridium complex encapsulated PEG-PLA nanoparticles used for imaging is 0.117 mg/mL).

CONCLUSION

The one-pot synthetic route for the mono cyclometalated iridium(III) complexes**1**-**12** that are strongly emissive in the solid state has been generalized. Tuning of the emission wavelength has been accomplished throughout the visible range through introduction of systematic changes in the chromophoric ligands. Quantum chemistry calculations at the DFT and TDDFT level have been used to explore the intricacies of the electronic natureof the ground and low-lying excited states involved in UV-vis absorption and photoemission processes confirming the experimental observations. Computed relative transition energies are in good agreement to measured absorption and emission peaks. Investigations were carried out to explore both the nature of the emitting states and the AIE activity for all these complexes. The dual functionalities exhibited by a common iridium(III) framework through proper selection and placement of the chromophoric (cyclometalating) and rotating entity (triarylphosphine) into the iridium(III) coordination sphere provide these molecules with interesting photophysical properties that can be exploited to obtain new cell imaging probes. To illustrate this possibility, the AIE active iridium(III) complex, **6** was encapsulated inside the hydrophobic core of PEG-PLA nanoparticles *via* the simple oil-in-water based emulsion-evaporation method. Aggregation of iridium complex molecules in the hydrophobic core of the PEG-PLA particles leads to an important increase of their emission intensity. The colloidal form of these luminescent PEG-PLA particles has been shown to behave as a potential cell imaging probe.

ASSOCIATED CONTENT

Time period for the syntheses of the complexes and their yield; crystal data and refinement, selected bond length and bond angles; IR, ^{1}H, ^{13}C and ^{31}P NMR spectra of the intermediates and complexes; PL emission spectra showing solvatochromic effect; DLS histogram for PEG-PLA; life-time data; bright field and luminescence image; comparison between X-ray and optimized geometries; computed vertical excitation energies to low-lying states, and computed emission wavelengths in solution. This material is available free of charge via the Internet at http://pubs.rsc.org.

AUTHOR INFORMATION

Corresponding Author
ir_laskar@bits-pilani.ac.in

ACKNOWLEDGMENT

We gratefully acknowledge the research funding from the 'Department of Science and Technology (DST), Govt. of India' and 'Council of Scientific and Industrial Research (CSIR), Govt. of India' for financial support under project Nos. SR/S1/IC-48/2009 (DST) and No. 01/2551/12/EMR-II (CSIR), respectively. We are also thankful to 'UGC-sponsored Special Assistance Programme (F.540/14/DRS/2007, SAP-I)' and DST FIST for instrumental support. Work in Barcelona was supported by MINECO-Spain (Project CTQ2011-23862-C02-02) and Generalitat de Catalunya (Projects 2009 SGR 1459and XRQTC). PD acknowledges CSIR India for providing a research fellowship. MK thanks DST for a fellowship.CC thanks MINECO-Spain for a predoctoral fellowship. We, also thank IISER Mohali for the use of their single crystal X-ray diffraction and NMR research facilities.

REFERENCE

1. (a) E. M.Linares, A.Formiga, L. T. Kubota, F.Galembeck and S.Thalhammer, *J. Mater. Chem. B*, 2013, **1**, 2236; (b) K.Yu, and K. S. Schanze, *ACS Appl. Mater. Interfaces*, 2013, **5**, 2785; (c) S. R.Stürzenbaum, M.Höckner, A.Panneerselvam, J. Levitt, J-S. Bouillard, S.Taniguchi, L-A. Dailey, Khanbeigi, R. Ahmad, E. V. Rosca, M.Thanou, K.Suhling and A. V. Zayats, Green, *M. Nat. NanoTech*., 2013, **8**, 57; (d) Y.Zhou, J.Jia, W.Li, H.Feia and M.Zhou, *Chem. Commun*., 2013, **49**, 3230; (e) X.Zhang, Z.Chi, Y.Zhang, S.Liu and J.Xu, *J. Mater. Chem. C*, 2013, **1**, 3376; (f) J. Y. Kim, T.Yasuda, Y. S. Yang and C. Adachi, *Adv. Mater*., 2013, (DOI: 10.1002/adma.201204902). (g) S. C. F. Kui, F-F. Hung, S-L Lai, M-Y Yuen, C-C.Kkok, K-H. Low, S. S-Y. Chui and C-M. Chi, *Chem.-A Eur. J.,* 2012, **18**, 96; (h) Q. Zhao, C.Huanga and F.Li, *Chem. Soc. Rev*., 2011, **40**, 2508; (i) Y.Chi and P.-T. Chou, *Chem. Soc. Rev*., 2010, **39**, 638; (j) S.Coe, W-K. Woo, M.Bawendi and V. Bulovic, *Nature*, 2002, 420, 800; (k) F. Hide, M. A. Díaz-García, B. J Schwartz, M. R.Andersson, Q.Pei and A. J. Heeger, *Science*, 1996, **273**, 1833; (l) H.Shi, J.Liu, J. Geng, B. Z. Tang and B. Liu *J. Am. Chem. Soc.,* 2012, **134**, 9569 − 9572; (m) W. Qin, D. Ding, J. Liu, W.Z.Yuan, Y.Hu, B. Liu, B. Z. Tang, *Adv. Funct. Mater.,* 2012, **22**, 771; (n) I. L. Medintz, H. T. Uyeda, E. R. Goldman and H. Mattoussi, *Nat. Mater*., 2005, **4**, 435; (o) L. Q. Xiong, Z. G. Chen, M. X. Yu, F. Y. Li, C. Liu and C. H. Huang, *Biomaterial*s, 2009, **30**, 5592; (p) R. P.Haugland, *A Guide to Fluorescent Probes and Labelling Technologies*, 10th ed.;Molecular Probes: Eugene, OR, 2005; (q) D.Wang, J. Qian, S. He, J. S. Park, K.-S. Lee, S. Han and Yi.Mu, *Biomaterials,* 2011, **32,** 5880.
2. (a) k. Slavı´, J. Fluorescence Microscopy and Fluorescent Probes, Plenum, New York, 1996; (b) B. Valeur, Molecular Fluorescence: Principle and Applications, *Wiley-VCH*, Weinheim, 2002.

3. (a) Advanced Concepts in Fluorescence Sensing, ed. C. D. Geddes and J. R. Lakopwicz, *Springer*, Norwell, 2005. (b) Fluorescence Sensors and Biosensors, ed. R. B. Thompson, CRC, Boca Raton, 2006.(c) W. H. Tan, K. M.Wang and T. J. Drake, *Curr. Opin. Chem. Biol*., 2004, **8**, 547; (d) K. E.Sapsford, L.Berti and I. L. Medintz, *Angew. Chem., Int. Ed.,* 2006, **45**, 4562; (e) S. M.Borisov and O. S. Wolfbeis, *Chem. Rev.*, 2008, **108**, 423.
4. (a) Y.Hong, J. W. Y.Lam and B. Z. Tang, *Chem. Commun*., 2009, 4332; (b) J.-S.Yang and J.-L. Yan, *Chem. Commun*., 2008, 1501; (c) Y.-T. Lee, C.-L. Chiang and C.-T. Chen, *Chem. Commun*., 2008, 217, (d) J.Wang, Y.Zhao, C. Dou, H.Sun, P. Xu, K .Ye, J.Zhang, S . Jiang, F.Li and Y.Wang, *J. Phys. Chem. B*, 2007, **111**, 5082; (e) C.-W.Wu, C.-M.Tsai and H.-C. Lin, *Macromolecules*, 2006, **39**, 4298; (f) S.-F.Lim, R. H. Friend, I. D. Rees, Li Y. J. Robinson, K.Ma, A. B.Holms, E.Hennebicq, D.Beljonne and F. Cacialli, *Adv. Funct. Mater*., 2005, **15**, 981; (g) F.He, Y.Tang, S.Wang, Y.Li and D.Zhu, *J. Am. Chem. Soc.*, 2005, **127,** 12343; (h) C.Fan, S.Wang, J. W.Hong, G. C. Bazan, K. W.Plaxco and A. J. Heeger, *Proc. Natl. Acad. Sci. U. S. A*., 2003, **100**, 6297; (i) S.Setayesh, A. C.Grimsdale, T.Weil, V.Enkelmann, K.Mu¨ llen, F.Meghdadi, E. J. W.List and G.Leising, *J. Am. Chem. Soc*., 2001, **123,** 946; (j) S.Hecht and J. M. J. Frechet, *Angew. Chem. Int. Ed*., 2001, **40**, 74; (k) R.Jakubiak, Z.Bao and L. Rothberg, *Synth. Met.,* 2000, **114**, 61; (l) A.Kraft, A. C. Grimsdale and A. B. Holmes, *Angew. Chem. Int. Ed*.,1998, **37**, 402.
5. (a) B. T.Nguyen, J. E.Gautrot, C.Ji, P.-L Brunner, M. T.Nguyen and X. X. Zhu, *Langmuir,* 2006, **22**, 4799; (b) A. P.Kulkarni and S. A.Jenekhe, *Macromolecules*, 2003, **36**, 5285; (c) S.Abe and L.Chen, *J. Polym. Sci. Part B: Polym. Phys*., 2003, **41,** 1676; (d) B. S.Gaylord, S.Wang, A. J.Heeger and G. C. Bazan, *J. Am. Chem. Soc*., 2001, **123**, 6417; (e) L.Chen, S.Xu, D.McBranch and D.Whitten, *J. Am. Chem. Soc*., 2000, **122,** 9302; (f) P. N.Taylor, M. J.O'Connell, L. A.McNeill, M. J. Hall, R. T.Aplin and H. L. Anderson, *Angew. Chem., Int. Ed.*,2000, **39**, 3456; (g) D.Sainova, T.Miteva, G.Nothofer, U.Scherf, I. Glowacki,. J. Ulanski, H.Fujikawa, and D. Neher, *Appl. Phys. Lett.*, 2000, **76**, 1810.
6. Y.Hong, J. W. Y.Lama and B. Z. Tang, *Chem. Soc. Rev***.,** 2011, **40**, 5361.
7. J.Luo, Z.Xie, J. W. Y.Lam, L.Cheng, H.Chen, C.Qiu, H. S.Kwok, X.Zhan, Y.Liu, D.Zhu and B. Z. Tang, *Chem. Commun.*, 2001, 1740.
8. (a) Z. Zhang, B. Xu, J.Su, L.Shen, Y.Xie and H.Tian*, Angew. Chem*., 2011, **123**, 11858 ; (b) S.Dong, Z.Li and J. Qin, *J. Phys. Chem. B*, 2009, **113**, 434; (c) Z.Xie, B.Yang, W. Xie, L. Liu, F.Shen, H.Wang, X.Yang, Z.Wang, Y.Li, M.Hanif, G.Yang, L.Ye and Y.Ma*, J. Phys. Chem. B,* 2006, **110**, 20993; (d) H. J. Tracy, J. L.Mullin, W.T.Klooster, J. A. Martin, J.Haug, S.Wallace, Watts Rudloe and K.I., *Inorg. Chem*., 2005, **44,** 2003; (e) Y.Ren, J. W. Y.Lam, Dong, Y. Y. B. Z. Tang, and K. S. Wong, *J. Phys. Chem. B*, 2005, **109,** 1135.
9. (a) N.Zhao, Y-H.Wu, J.Luo, L-X.Shia and Z-N Chen, *Analyst*, 2013, **138**, 894; (a) H.Wu, T.Yang, Q.Zhao, J.Zhou, C.Lia and F.Li, *Dalton Trans*.,2011**, 40,** 1969; (b) G-G.Shan, D-X. Zhu, H-B. Li, P.Li, Z-M.Su and Y.Liao, *Dalton Trans.,* 2011, **40**, 2947; (c) Q.Zhao, L.Li, F.Li, M.Yu, Z.Liu, T.Yi and C.Huang, *Chem.Commun.,* 2008, 685; (d) Y.You, H. S.Huh, K. S.Kim, S. W.Lee, D.Kim and S. Y.Park*, Chem. Commun*., 2008, 3998.
10. C. Xu, Z-Q.Wang, X-M.Dong, X-Q.Hao, X-M.Zhao, B-M.Ji and M-P. Song, *Inorg. Chim. Acta*, 2011, **373**, 306.
11. P.Alam, M.Karanam, A. R.Choudhury, I. R. Laskar, *Dalton Trans*., 2012, **41**, 9276.
12. G.Ruana and S-S. Feng, *Biomaterials* , 2003, **24,** 5037.
13. APEX2;SADABS; SAINT; Bruker AXS Inc.: *Madison, Wisconsin, USA,* 2008.
14. G. M. Sheldrick, *Acta Crystallogr. A*. 2008, **64**, 112.
15. O. V.Dolomanov, L. J.Bourhis, R. J.Gildea, Howard, J. A. K.Puschmann and H. *J., Appl. Cryst*. 2009, **42**, 339.
16. Nardelli, M. *J. Appl. Cryst*. 1995, **28,** 659.
17.S. Grimme, *J. Comp. Chem*., 2006, **27**,1787.
18. (a) P.J.Hay and W.R. Wadt, *J. Chem. Phys*., 1985, **82**, 270. (b) W.R.Wadt and P.J. Hay, *J. Chem. Phys*., 1985, **82**,284. (c) P.J.Hay, and W.R. Wadt, *J. Chem. Phys*., 1985, **82** 299. (d) P.C. Hariharan and Pople, *J.A. Mol. Phys*., 1974**, 27**,209.
19. (a) C.Lee, W.Yang and R.G. Parr*, Phys. Rev. B*, 1988, **37** 785. (b) A.D. Becke, *J. Chem. Phys*., 1993, **98** 5648.
20. (a) E. Cancès, B. Mennucci, J. Tomasi,*J. Chem. Phys.,*1997, **107**3032; (b) B. Mennucci, E. Cancès, J. Tomasi, *J. Phys. Chem. B, 1997,* **101**, 10506; (c)E. Cancès, B. Mennucci, *J. Math. Chem.* 1998,**23**, 309.
21.Gaussian 09 Revision B.01, Frisch, M.J.et al., Gaussian, Inc., Wallingford, CT, 2009.
22. H. D.Kaesz and R. B. Saillant, *Chem. Rev.,* 1972, **72**, 231.
23. M. A.Bennett and D. L. Milner, *J. Am. Chem. Soc.*, 1969, **91**, 6983.
24. (a) C-H.Chang, C-L.Ho, Y-S.Chang, I-C.Lien,C.-H.Lin, Y-W. Yang, J-L. Liao and Y.Chi, *J. Mater. Chem. C*, 2013, **1**, 2639. (b) C-H.Yang, S-W.Li, Y. Chi, Y-M.Cheng, Y-S.Yeh, P-T.Chou, G-H.Lee, C-H.Wang and C-F. Shu, *Inorg. Chem*., 2005, **44**, 7770.
25. (a) I. R.Laskar, S-F.Hsu and T-M.Chen, *Polyhedron*, 2005, **24**, 189.(b) S.Lamansky, P.Djurovich, D.Murphy, F.Abdel-Razzaq, R.Kwong, I.Tsyba, M.Bortz, B.Mui, R.Bau and M. E. Thompson, *Inorg. Chem*., 2001, **40**, 1704.
26. J. C. de Mello, H. F. Wittmann and R. H. Friend, *Adv. Mater.,* 1997, **9**, 230.
27. Y.Ren, J. W. Y.Lam, Y.dong, B. Z.Tang and K. S. J. Wong, *Phys. Chem. B,* 2005, **109,** 1135.
28. R. Z.Xiao, Z. W.Zeng, G. L.Zhou,J. J. Wang, F. Z.Li andA. M. Wang, *Int J Nanomed.,*2010, **5,** 1057.
29. Q.Wang, Y.Bao, J.Ahire and Y.Chao, Adv. Healthcare Mater., 2012, DOI: 10.1002/adhm.201200178.
30. A. M.Talarico, M.Ghedini, C. O.Rossia and E. I. Szerb*, Soft Matter*, 2012, **8**, 11661.
31. Nikhil R. Jana, *PhysChemChemPhys.*, 2011, **13**, 385.

Facile Tuning of the Aggregation Induced Emission Wavelength in a Common Framework of a Cyclometalated Iridium(III) Complex : Micellar Encapsulated Probe in Celluler Imaging

Parvej Alam[a], Pradip Das[b], Clàudia Climent[c], Maheswararao Karanam[d], David Casanova[c], Angshuman Roy Choudhury[d]*, Pere Alemany[c]*, Nikhil R. Jana[b]*, Inamur Rahaman Laskar[a]*

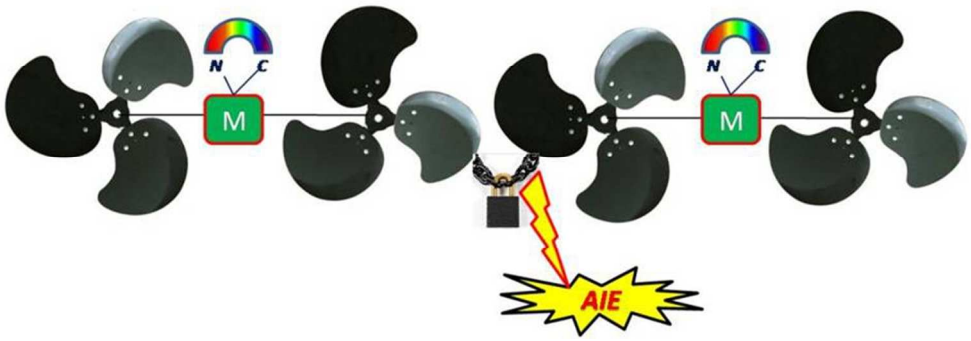

163x59mm (150 x 150 DPI)